The response of tropical precipitation to Earth's precession: The role of fluxes and vertical stability

Chetankumar Jalihal[1,3], Joyce Helena Catharina Bosmans[2], Jayaraman Srinivasan[3], and
Arindam Chakraborty[1,3]

[1]Centre for Atmospheric and Oceanic Sciences, Indian Institute of Science, Bangalore, India
[2]Department of Environmental Science, Radboud University, The Netherlands
[3]Divecha Centre for Climate Change, Indian Institute of Science, Bangalore, India

Correspondence: Chetankumar Jalihal (jalihal@iisc.ac.in)

Abstract.

The changes in Earth's precession have an impact on tropical precipitation. These changes have been ascribed to the changes in solar radiation at the top of the atmosphere, but this cannot explain the variations in precipitation over oceans. Using energy and moisture budget equations we have shown that the surface energy fluxes, as well as vertical stability, have to be taken into
5 consideration along with insolation, to explain these changes in precipitation. Energy fluxes explain most of the changes in precipitation, when looking at the mean response over the tropics. However, there are regions like the Arabian sea and Africa where stability change is the main cause of change in precipitation. Hence, insolation cannot be thought of as the sole driver of precipitation on orbital timescales, but surface energy and vertical stability should also be considered when looking at oceans or smaller land regions. The decrease in precipitation over the Bay of Bengal, with higher summer insolation, has been shown
10 to be due to the decrease in surface latent heat fluxes. This is a consequence of the remote response of the atmosphere to the enhanced latent heating to the west of Bay of Bengal. This leads to a decrease in wind speed over the Bay of Bengal and hence reduces the total column energy available for convection.

1 Introduction

15 Using speleothem records, past studies have shown that the intensity of monsoon is directly proportional to insolation on orbital timescales (Wang et al., 2007, 2008; Cruz Jr et al., 2005). The model based studies suggest, however, that while this is true over land, the precipitation over tropical oceans is in general, inversely related to insolation (Clement et al., 2004; Tuenter et al., 2003; Chamales, 2014). For example, the summers of Mid-Holocene (MH), had about 20 W/m^{2} more insolation over India, than the present day summer. An increase in summer rainfall can be found in the proxies (Ramesh, 2001; Patnaik et al., 2012;
20 Zhang et al., 2016). The simulations of the MH monsoon by climate models indicate that the precipitation over Bay of Bengal

(BoB) was less (Hsu et al., 2010; Bosmans et al., 2012; Zhao and Harrison, 2012). The India-BoB asymmetry, is a regional manifestation of the land-ocean asymmetry in the response of precipitation to changes in the Earth's precession.

This has been explained in the previous studies using the *land-sea thermal contrast theory* of the monsoon (Zhao and Harrison, 2012; Bosmans et al., 2012). According to this theory, with increased insolation land warms more than the surrounding ocean, because of its lower thermal inertia. This increases the land-sea thermal contrast in surface temperature. However, the thermal contrast disappears after the onset of monsoon due to cooling of land by precipitation and cloud cover. In fact, good monsoon years have a lower land surface temperature (Gadgil, 2018).

The other mechanism that has been proposed is the *slow ocean response theory* (Braconnot et al., 2000; Hsu et al., 2010). The ocean, due to its higher heat capacity, takes about a month or two to respond to the insolation forcing. However, there are still many oceanic regions where, precipitation responds differently. This indicates that local processes are dominant in those regions. Thus the slow ocean response while true in general, may not explain precipitation response in small basins like the Bay of Bengal.

Some studies have used the energy balance to explain the response of precipitation to precession (Braconnot et al., 2008; Hsu et al., 2010; Merlis et al., 2013; Chamales, 2014; Battisti et al., 2014). While Braconnot et al. (2008) suggested a possible connection between changes in precipitation and changes in divergence of Moist Static Energy (MSE), Chamales (2014) and Merlis et al. (2013) have shown how they are connected using a theoretical framework. The analysis done by Merlis et al. (2013) is for the zonal mean, and this does not reflect the actual conditions in a full General Circulation Model (GCM) with continents. Hsu et al. (2010) found in their model of intermediate complexity that the changes in vertical velocity, which are in turn a response to changes in total column energy drive the changes in precipitation. This is again a tropical mean picture and regional response might be different from the tropical mean response. Also, a quantitative estimate of the parameters governing changes in precipitation is missing. Battisti et al. (2014) focused on the asymmetry between central India and Bay of Bengal, and suggested that higher summer insolation causes the near surface energy to migrate from the Bay of Bengal to India. But as shown in the appendix A, our climate model does not show such a migration in near surface energy. We propose an alternative model based on total energy in a column and stability of the column to explain the changes in precipitation in all regions of the tropics in response to changes in Earth's precession.

In this paper we have used a high-resolution, state-of-the-art fully coupled model EC-Earth in two orbital configurations, which correspond to the extremes in precession. The advantage of doing this is that, it has a similar spatial precipitation response as observed in MH, but with higher amplitude. This paper is organized as follows. The next section describes the model and the experimental setup. Section 3 outlines a simple model for the Inter Tropical Convergence Zone (ITCZ) that we have used to interpret the results. The results are described in section 4 followed by discussion and conclusions.

2 Model and experimental details

EC-Earth is a fully coupled ocean-atmosphere GCM, (Hazeleger et al., 2010, 2012). The model version 2.2 where, Integrated Forecasting System (IFS) is the atmospheric component was used. It has a spectral resolution of T159 (roughly 1.125º x

1.125º) with 62 vertical levels. The convective scheme Bechtold et al. (2008) is used along with the Balsamo et al. (2009) land surface scheme H-TESSEL, including surface runoff. The version 2 of Nucleus for European Modeling of the Ocean (NEMO) forms the ocean component. It has a horizontal resolution of 1º with 42 vertical levels (Madec, 2008; Sterl et al., 2012). NEMO includes sea-ice model LIM2. OASIS3 coupler Valcke and Morel (2006) couples the ocean, sea-ice, land and

5 atmosphere. EC-Earth performs well for the present day when compared to CMIP3 models in terms of climatology as well as inter-annual, spatial and temporal variability (Hazeleger et al., 2010, 2012).

Earth's precession with a period of 23,000 years, is the most dominant mode in insolation as well as in tropical precipita- tion. The two precession extremes, Precession minima: P_{min} and Precession maxima: P_{max}, correspond to summer solstice at perihelion and winter solstice at perihelion respectively (Figure 1). Table 1, shows the orbital configurations used. This causes

10 a stronger seasonal cycle in the Northern Hemisphere (NH) and a weaker seasonal cycle in Southern Hemisphere (SH), in P_{min} (Figure 2). The opposite occurs during a P_{max}.

The model is run separately for each of the orbital configurations. The length of each simulation is 100 years, with the first 50 years being considered as spin-up. The last 50 years are used to generate climatology. All analysis has been done with this climatological data. The orbital parameters remain constant throughout the simulation. All other boundary conditions (e.g. the

15 solar constant, greenhouse gas con- centrations, orography, ice sheets, vegetation) were kept constant at pre-industrial levels. Vernal equinox has been fixed at 21st March, and the present day calendar is used. But since the length of season and the dates of equinoxes change along the precesssion cycle, the autumn equinoxes do not coincide. This is known as the *Calendar Effect*. It introduces some errors due to phasing of insolation. We do not make any corrections in order to be consistent with previous studies. For further details about the experiments see Bosmans et al. (2015).

20 **3   A simple model for ITCZ**

Hadley cell is a thermally direct, overturning circulation in the tropics. It takes energy away from the tropics and towards the poles. The Hadley cell has a rising branch in the deep tropics and a descending branch in the extra-tropics. This leads to moisture convergence near the rising branch. ITCZ coincides with the rising branch of the Hadley cell, and is responsible for the zone of heaviest precipitation in the tropics. Since, the Hadley cell is governed by energy and leads to moisture convergence,

25 the characteristics of ITCZ can be described by using the conservation equations for Moist Static Energy (MSE) and moisture. Using this approach, Neelin and Held (1987) proposed a simple model for ITCZ in terms of net energy input into the atmosphere and vertical stability. This is a diagnostic model, that has been used to explain variations in rainfall due to global warming (Chou and Neelin, 2004; Chou et al., 2006) and the impact of aerosols (Chou et al., 2005) . In this section we have discussed this simple model in detail.

The equations 1 and 2 correspond to the conservation of MSE and moisture in a vertical column of the atmosphere. Refer to Neelin and Held (1987) for further details on the derivation of equation 1. The time derivatives have been dropped in these equations because, the climate is assumed to be in a steady state. The angle brackets ($< >$) indicate vertical integral.

$$\langle \nabla \cdot m\boldsymbol{U} \rangle + \left\langle \frac{\partial m\omega}{\partial p} \right\rangle = Q_{div} \tag{1}$$

$$\langle \nabla \cdot q\boldsymbol{U} \rangle + \left\langle \frac{\partial q\omega}{\partial p} \right\rangle = E - P \tag{2}$$

$$\langle A \rangle = - \int_{P_b}^{P_t} A \frac{dp}{g} \tag{3}$$

where,

P - Precipitation (mm/day)

E - Evaporation (mm/day)

10   Q_{div} - Total Column Energy .i.e. the sum of all the fluxes into the atmosphere at the top and bottom of the atmosphere. (in mm/day; 1 mm/day = 26.16 W/m^2). Over land, since the storage term is small, the sum of all the fluxes of energy at the surface is small. Hence, Q_{div} is mainly governed by the fluxes at the Top of Atmosphere (TOA). However, over oceans the contribution of surface fluxes is large.

q - specific humidity (Kg/Kg)

15   m – Moist Static Energy, which is the sum of internal energy, potential energy and moist energy ($C_pT + gZ + L_vq$)

P_b – Pressure at the bottom of the atmospheric column

P_t – Pressure at the top of the atmospheric column

g – acceleration due to gravity

20   Assuming $\omega = 0$ at the top as well as the surface, leaves us with the horizontal terms only. The governing equations can be combined and simplified (equation 4).

$$P - E = \frac{Q_{div}}{GMS} \tag{4}$$

$$GMS = \frac{m_1 - m_2}{L_v(q_2 - q_1)} \tag{5}$$

$$m_1 = \frac{\displaystyle\int_{P_t}^{P_m} m \nabla \cdot \boldsymbol{U} dp/g}{\displaystyle\int_{P_t}^{P_m} \nabla \cdot \boldsymbol{U} dp/g} \qquad (6)$$

$$m_2 = \frac{\displaystyle\int_{P_m}^{P_b} m \nabla \cdot \boldsymbol{U} dp/g}{\displaystyle\int_{P_m}^{P_b} \nabla \cdot \boldsymbol{U} dp/g} \qquad (7)$$

where,

GMS is the Gross Moist Stability, as obtained by taking the ratio of the equations 2.11 and 2.12 from (Neelin and Held, 1987).

5   m_1 and m_2 are respectively, the total MSE in the upper (mid-troposphere to top) and lower troposphere (surface to mid-troposphere), normalized by divergence of that layer. Thus GMS is mainly a function of vertical profiles of MSE.

P_m - Pressure at mid-troposphere level

Similarly, q_1 and q_2 represent the total moisture in the upper and lower troposphere, normalized by divergence. The mass convergence in the lower troposphere is the same as the mass divergence in the upper troposphere. Here (Neelin and Held,

10   1987) assume that the horizontal gradients of temperature and moisture are weak within the tropics. This implies that the horizontal advection of temperature and moisture are small. This simple model attributes the changes in (P-E) to either the changes in total column energy or the vertical stability.

     Figure 3 shows a scatter of (P-E) as a function of Q_{div} for the three summer months JJA taken separately. The scatter is made for Central India, BoB and North Africa for each of the precession extremes. We chose these three regions to highlight that

15   neglecting the role of advection, may not always be appropriate. The plot shows that the two are nearly linear, as predicted by the simple model (equation 4). The slight deviations from linearity are due to variations in GMS. As we go from P_{max} to P_{min} (low to high insolation in NH summer months), both Q_{div} and (P-E) increase over Central India and North Africa (land regions). However, both these quantities decrease over BoB (oceanic region). Being the summer months, Q_{div} is positive for all these regions.

20   To further look at the role of GMS we have shown in figure 4, a scatter of (P-E) vs GMS for the same three regions and months. There is no definite relation between the two. Based on equation 4, we would expect all positive values for GMS since, (P-E) and Q_{div} are both positive. But there are some points where GMS is negative. This indicates that the assumption about the horizontal advection terms being small is not always valid. Hence, we need to modify the definition of GMS to include horizontal advection terms.

By taking the ratio of equations 1 and 2, after multiplying equation 2 by L_v (the latent heat of vaporization for water), we get:

$$P - E = \frac{Q_{div}}{TGMS} \tag{8}$$

$$TGMS = \frac{\left\langle \nabla \cdot m\boldsymbol{U} + \frac{\partial m\omega}{\partial p} \right\rangle}{L_v \left\langle \nabla \cdot q\boldsymbol{U} + \frac{\partial q\omega}{\partial p} \right\rangle} \tag{9}$$

5   Where,

TGMS stands for Total GMS (the term "Total" indicates inclusion of all advection terms).

TGMS, has only one assumption built into it: the time derivatives of m and q are very small. This is a good assumption for a steady state climate. TGMS is particularly useful for smaller regions, where horizontal advection can be large. TGMS represents how efficiently an atmospheric column can diverge MSE per unit moisture converged into the column. This suggests

10   that, along with the vertical profile of MSE, the amount of energy taken out of the column and the amount of moisture going into the column might be important. Since we are using climatological data, the errors in the calculations of TGMS were significant. Hence, we use the equivalence in equation 1 and 2, to estimate TGMS. Since, our goal is not to estimate the changes in (P-E), but to diagnose the cause of these changes, estimation of TGMS this way, can be justified.

4   Results

15   In this section we have discussed the relative importance of Q_{div} and TGMS in explaining the changes in (P-E) between P_{min} and P_{max}. First we start by giving an overview of the entire tropics and then we look at the peculiar case of the Indian subcontinent in detail.

4.1   Tropics

4.1.1   Qualitative analysis

20   Figure 5 shows the difference in precipitation between P_{min} and P_{max}, averaged over tropical land and oceans separately. Precipitation change over tropical land is out of phase with the changes in precipitation over the oceans. Amplitude of the change is higher over land than over oceans. Also note that larger change in precipitation over land, occurs during boreal summer when compared to austral summer. This implies that the northern monsoons are more sensitive to precession than southern monsoons. Since, for both the orbital configurations Vernal equinox occurs on the same date (21st March), the difference in

25   insolation between the two cases is very small during March. Hence, the precipitation response is also similar. Therefore the changes in land and ocean precipitation has a zero crossing during this month. Since, the quantity of interest to us is (P-E), from here onwards, all of our analysis concerns (P-E) instead of just precipitation.

In figure 6, is shown a spatial pattern of the changes in (P-E) and Q_{div} averaged over JJA (left panels) and DJF (right panels). First we discuss the response during JJA. Most of the land regions in the northern hemisphere show an increase in (P-E) and. The African monsoon is much stronger in P_{min} with an increase of about 10 mm/day. (P-E) has in general decreased over oceans. However, there are many regions over oceans where (P-E) has increased. Ocean has a much more heterogeneous

5 response in comparison to land. This explains why the amplitude of the changes in (P-E) is small when averaged over all of the tropical oceans (figure 5).

Changes in Q_{div} having a strikingly similar spatial pattern to that of (P-E), with positive values over most of the land regions, and both positive and negative values over oceanic regions. This shows again the direct relation of (P-E) to Q_{div} as suggested by the simple model. However, there are some exceptions like the Arabian sea where, Q_{div} has decreased but (P-E) has increased.

10 Also the region of maximum increase in (P-E) and Q_{div} are not co-located over Africa. This is on account of the changes in TGMS.

During DJF, P_{min} has lesser insolation (Figure 2) and correspondingly a decrease in (P-E) and Q_{div} is seen over land regions (Figure 6 c and d). Oceans show a heterogeneous response during DJF as well. Even though, the magnitude of changes in Q_{div} are of the same order as in JJA, the changes in (P-E) are much less in DJF as compared to JJA.

15 ### 4.1.2 Quantitative analysis

To quantify the relative dominance of Q_{div} and TGMS in explaining the changes in (P-E), we do the following. Writing equation 8 for P_{max}:

$$P - E = \frac{Q}{G} \tag{10}$$

where,

20 P, E, Q and G are precipitation, evaporation, Q_{div} and TGMS respectively. Considering P_{max} as the reference case and P_{min} as the perturbed case, we can write the following for P_{min}:

$$(P + \Delta P) - (E + \Delta E) = \frac{Q + \Delta Q}{G + \Delta G} \tag{11}$$

Where Δ represents the perturbation from P_{max}. Now dividing by (P-E), we get

$$1 + \frac{\Delta(P-E)}{(P-E)} = \frac{1 + \Delta Q/Q}{1 + \Delta G/G} \tag{12}$$

25 This equation can further be modified as:

$$\underbrace{\Delta(P-E)}_{\text{Change in P-E}} = \underbrace{\frac{\frac{\Delta Q}{Q}}{1 + \frac{\Delta G}{G}}(P-E)}_{\text{Contribution from } Q_{div}} + \underbrace{\frac{-\frac{\Delta G}{G}}{1 + \frac{\Delta G}{G}}(P-E)}_{\text{Contribution from TGMS}} \tag{13}$$

Now we apply the above equation to different regions in the tropics (Figure 7). The top panel is for regions in the northern hemisphere and the bottom panel is for the southern hemipshere. The analysis was done for the summer months of the respective hemispheres (JJA for northern and DJF for the southern hemisphere). The blue stick represents the changes in (P-E), whereas the red and orange sticks are contributions from Q_{div} and TGMS. Q_{div} explains most of the changes in (P-E) over all of the

5   land regions in northern tropics. This is however, a generalization because, TGMS contributes most to the changes in (P-E) over Africa. Because of the heterogeneous response of (P-E) over oceans, the fractional change in (P-E) is very small and the contributions from Q_{div} and TGMS are in opposite directions, thus cancelling each other out. BoB shows a decrease in (P-E) most of which is explained by changes in Q_{div} with the changes in TGMS being very small.

The southern tropics has a dominant contribution from Q_{div} over both land and oceans. However, some of the regions shown

10   either have an equal contribution from TGMS (South Africa and Brazil) or TGMS is the dominant cause of the changes in (P-E) (North Australia and South Atlantic). Figure 7, highlights that the tropical mean response is not representative of regional responses. Hence, each region has to be studied separately to understand the physical mechanism that caused the changes in (P-E). Of particular interest is the Indian monsoon. Both BoB and Indian landmass are part of this monsoon, yet they have opposite response to precessional forcing. Hence, we discuss this asymmetric response of Indian monsoon in detail, in the

15   following subsection.

4.2 The Indian monsoon

From figure 7a, we have established that the increase and decrease of (P-E) over India and BoB respectively was due to Q_{div}. Here we examine in detail, what caused these changes in Q_{div}. We look at each of the fluxes at the surface and Top of Atmosphere (TOA) separately:

20   $$Q_{div} = \underbrace{LHF + SHF + Net\_Sfc\_Rad}_{\text{bottom fluxes}} + \underbrace{Net\_TOA\_LW + Net\_TOA\_SW}_{\text{TOA Fluxes}} \qquad (14)$$

Where,

LHF : Surface Latent Heat Flux

SHF : Surface Sensible Heat Flux

Net_Sfc_Rad = Net Surface Radiation (Long wave + Short wave)

25   Net_TOA_LW : Net Top Of Atmosphere Long wave radiation

Net_TOA_SW : Net Top Of Atmosphere Short wave radiation

Clubbing together all the radiation fluxes into one quantity Q_{rad}, we get:

$$Q_{div} = LHF + SHF + Q_{rad} \qquad (15)$$

Figure 8, is a spatial map of the differences in (P-E), Q_{div} and its components. Q_{div} has a good spatial coherence with (P-E), over most of the regions except Arabian sea. As was discussed earlier, changes in TGMS drive the changes in (P-E) over Arabian sea. Also note that (P-E) has decreased along the southern parts of the western ghats, but has increased in the northern extent of the Western Ghats. Q_{rad} bears a better resemblance to (P-E). This suggests that radiative feedbacks from clouds are
5   present. But these feedbacks are not able to counter the large decrease in Latent Heat Flux (LHF) over Arabian sea and BoB. This makes Q_{div} decrease over these regions. In fact Q_{div} and LHF have similar spatial patterns over the oceanic regions. The changes in Sensible Heat Fluxes (SHF) are small in most places.

To establish quantitatively, what drives changes in Q_{div}, we take two regions one over Central India (15°-25^oN; 73°-83^oE) and the other over BoB (10°-20^oN; 85°-95^oE). These regions are shown as black boxes in Figure 8a. The changes in the three
10   components of Q_{div}, over these two regions is shown in the barchart (Figure 8f). It shows the dominance of the radiative terms over India and LHF over BoB.

LHF is a function of surface wind speed, Sea Surface Temperature (SST) and how close the atmosphere is to saturation. LHF increases with increase in wind speed and SST. However, SST has increased over BoB and Southern Arabian sea by about 2^oC (not shown). Hence, we look at the changes in wind speed (Figure 9). The top panel of Figure 9 (a and b) show the JJA mean
15   winds at 850 hPa. The shading indicates wind speed and the unit vectors the direction. The axis of the Low Level Jet (LLJ) has shifted to the north and this has caused decrease in winds over BoB. Due to LLJ, deep oceanic water upwells along the coast of Somalia. This makes the SST over western parts of Arabian sea colder. However, due to the northward shift of the LLJ, the region of upwelling also shifts north, leading to cooler SSTs in the Northern Arabian sea. Thus the decrease in LHF over Arabian sea is due to weaker winds in the southern parts and colder SST in the northern parts.

20   Also the shift in LLJ leads to lesser moisture flux along the southern part of the Western Ghats. Hence, the decrease in (P-E). At the same time the LLJ now brings more moisture into the northern parts of Western Ghats, leading to increase in (P-E). The shift of the LLJ can be seen more clearly in Figure 9c, where the difference in winds between P_{min} and P_{max} is shown. There is a low level easterly along the equatorial Indian ocean and a low level westerly over the African landmass, also along the equator. These two low level winds converge near the eastern coast of Africa, at around longitude 40^oE. Also on the same
25   meridian is a cyclonic circulation to the north, situated over the Middle-East and an anti-cyclonic circulation to the south, over Madagascar. This resembles the Gill-like response of the atmosphere to heating of an atmospheric column (Gill, 1980).

(Gill, 1980) proposed a simple shallow water model on an equatorial β plane to understand the role of latent heating on surface winds. He put heat sources in different regions, to heat the entire atmospheric column over these regions. This was meant to represent convective heating due to latent heat release. When this model was forced with heating over a region at
30   equator and another region off-equator, it produced a Kelvin wave along the equator and a Mixed Rossby-Gravity wave which had a cyclonic and an anti-cyclonic circulation in the northern hemisphere and southern hemisphere respectively. The Kelvin wave causes low level convergence along the equator, over the region of equatorial heat source. The wind response of our model, hence suggests that the wind patterns over the Indian subcontinent, are driven by atmospheric heating near equator and off-equator. Examining figure 6a, will show that the heat sources correspond to convective heating of the column due to
35   increased precipitation over the West Equatorial Indian Ocean (WEIO) and over the Red sea. The convection over the Red sea,

is part of the African monsoon which has extended into this region. There are however, some important differences between our model and the Gill model. Ours a full GCM with non-zero mean background winds, whereas Gill model has zero mean background winds. This implies that our model response includes non-linear terms.

To summarize, the decrease in Q_{div} over BoB, is due to decreased winds over BoB. The winds decrease on account of a remote response to convective heating over WEIO and the Red Sea. The next question we want to address is, what factors lead to increased convection over these regions. To understand this, we look at the month of May, even before the Indian monsoon circulation has set up. Figure 10a and b, show the difference in Q_{div} and (P-E) for the month of May. The shading in figure 10b is for (P-E) and the unit vectors represent the changes in wind direction. Q_{div} is higher over Africa, and this causes early onset of monsoon (Figure 10b). Thus changing the low level winds along the eastern coast of Africa. This leads to reduced upwelling and increased SST. With increased SST, convection begins and this further enhances the low level convergence. This positive feedback is responsible for the convective heating over the WEIO. As the African monsoon progresses north, the region of convection over the eastern side of Africa moves over to the Red sea. This becomes the off-equatorial heat source.

5 Discussion and conclusions

Models with different levels of complexities: QTCM (Hsu et al., 2010), Quasi-geostrophic model EC-Bilt (Tuenter et al., 2003), GCM with slab ocean (Battisti et al., 2014) and finally the fully coupled model EC-Earth (Bosmans et al., 2018), have all shown the land-sea asymmetry in precipitation, when subjected to precessional forcing. Also the land-sea asymmetry exists irrespective of the details of the orbital configuration (Mid-holocene, or idealized experiments). This suggests that the asymmetry is on account of a very fundamental mechanism. We agree with the previous studies that this is on account of the *slow ocean response*. However, changes in precipitation over ocean are not of the same sign everywhere (Figure 6a). In fact ocean has a more heterogeneous response than land, suggesting that the role of local processes dominates over the slow ocean response in these regions. Hence, it is necessary to study smaller regions, separately to understand the precipitation response (Figure 7).

We have analysed and interpreted the response of a high resolution fully coupled model EC-Earth, to precession, by using a simple model, based on the conservations of energy and moisture. With the help of the simple model, we can diagnose the changes in precipitation, in terms of two variables .viz. the total energy going into the column (Q_{div}) and the vertical stability of the atmosphere (GMS). We have included the horizontal advection terms which were originally assumed small (Neelin and Held, 1987). This allows us to use the simple model for relatively smaller domains, where horizontal advection terms can be large. We find that precipitation changes between precession extremes, are in general, due to changes in Q_{div}. Insolation drives changes in Q_{div} over land, whereas latent heat fluxes contribute most over oceans. Particularly, the changes in winds over the Bay of Bengal, cause latent heat fluxes to decrease. These changes in wind speed are associated with convecting heating of the atmospheric column over the west equatorial Indian ocean and the Red sea.

EC-Earth does get an increase in precipitation over the Indian landmass for minimum precession (higher summer insolation), consistent with the proxy records (Kathayat et al., 2017). However, there are no proxies for precipitation over oceanic regions.

As we move further back in time (through the Holocene), we move closer to a minimum precession configuration. This means higher summer insolation and lower winter insolation than the present day. Hence, we would expect precipitation to decrease over the Bay of Bengal as we move further back in time, through the Holocene. A speleothem chronology from the Baratang cave in the Andaman islands (Laskar et al., 2013), can be thought of as a representation of precipitaion over the Bay. This

5   chronology goes back to 4,000 years before present, and shows a long-term decreasing trend in precipitation. This suggests that the EC-Earth is doing well in capturing the land-sea asymmetry between India and Bay of Bengal.

There are however, regions where changes in stability is the main cause of changes in precipitation (eg. Africa and Arabian sea). Stability (the Gross Moist Stability) is based on the coupling between the divergence of moisture and moist static energy fluxes. This suggests that between the precession extremes, this coupling had changed. Why it changes so, requires further

10   investigation.

Appendix A

For orbital configuration with higher summer insolation, the rate of increase in surface temperature is high over India (due to lower thermal heat capacity). Battisti et al. (2014) suggested that this causes near surface MSE to be higher over India. It is known that the location of ITCZ coincides with that of the surface MSE (Bordoni and Schneider, 2008). Hence ITCZ migrates

15   over India quickly and remains there. However, our plot of near surface equivalent potential temperature, θ_e (same as near surface MSE), suggests that BoB has higher energy all throughout the year for both the precession extremes (Figure A1).

Author contributions. Dr. J.H.C Bosmans designed and ran the experiments. Mr. Chetankumar Jalihal, Prof. Jayaraman Srinivasan, and Prof. Arindam Chakraborty analyzed and interpreted the GCM output.

Competing interests. The authors declare that they have no conflict of interest.

20   *Acknowledgements.* We acknowledge support from the Centre for Excellence in the Divecha Centre for Climate Change (DCCC). This work was partially funded by DST India.

References

Balsamo, G., Beljaars, A., Scipal, K., Viterbo, P., van den Hurk, B., Hirschi, M., and Betts, A. K.: A revised hydrology for the ECMWF
model: Verification from field site to terrestrial water storage and impact in the Integrated Forecast System, Journal of hydrometeorology,
10, 623–643, 2009.

5 Battisti et al.: Coherent pan-Asian climatic and isotopic response to orbital forcing of tropical insolation, Journal of Geophysical Research:
Atmospheres, 119, 2014.

Bechtold, P., Köhler, M., Jung, T., Doblas-Reyes, F., Leutbecher, M., Rodwell, M. J., Vitart, F., and Balsamo, G.: Advances in simulating
atmospheric variability with the ECMWF model: From synoptic to decadal time-scales, Quarterly Journal of the Royal Meteorological
Society, 134, 1337–1351, 2008.

10 Bordoni, S. and Schneider, T.: Monsoons as eddy-mediated regime transitions of the tropical overturning circulation, Nature Geoscience, 1,
515, 2008.

Bosmans et al.: Monsoonal response to mid-holocene orbital forcing in a high resolution GCM, Climate of the Past, 8, 723, 2012.

Bosmans, J., Drijfhout, S., Tuenter, E., Hilgen, F., and Lourens, L.: Response of the North African summer monsoon to precession and
obliquity forcings in the EC-Earth GCM, Climate dynamics, 44, 279–297, 2015.

15 Bosmans, J., Erb, M., Dolan, A., Drijfhout, S., Tuenter, E., Hilgen, F., Edge, D., Pope, J., and Lourens, L.: Response of the Asian summer
monsoons to idealized precession and obliquity forcing in a set of GCMs, Quaternary Science Reviews, 188, 121–135, 2018.

Braconnot et al.: Ocean feedback in response to 6 kyr BP insolation, Journal of Climate, 13, 1537–1553, 2000.

Braconnot et al.: Monsoon response to changes in Earth's orbital parameters: comparisons between simulations of the Eemian and of the
Holocene, Climate of the Past Discussions, 4, 459–493, 2008.

20 Chamales, K. A.: The effects of orbital precession on tropical precipitation, 2014.

Chou, C. and Neelin, J. D.: Mechanisms of global warming impacts on regional tropical precipitation, Journal of climate, 17, 2688–2701,
2004.

Chou, C., Neelin, J. D., Lohmann, U., and Feichter, J.: Local and remote impacts of aerosol climate forcing on tropical precipitation, Journal
of climate, 18, 4621–4636, 2005.

25 Chou, C., Neelin, J. D., Tu, J.-Y., and Chen, C.-T.: Regional tropical precipitation change mechanisms in ECHAM4/OPYC3 under global
warming, Journal of Climate, 19, 4207–4223, 2006.

Clement, A. C., Hall, A., and Broccoli, A.: The importance of precessional signals in the tropical climate, Climate Dynamics, 22, 327–341,
2004.

Cruz Jr, F. W., Burns, S. J., Karmann, I., Sharp, W. D., Vuille, M., Cardoso, A. O., Ferrari, J. A., Dias, P. L. S., and Viana Jr, O.: Insolation-
30 driven changes in atmospheric circulation over the past 116,000 years in subtropical Brazil, Nature, 434, 63, 2005.

Gadgil, S.: The monsoon system: Land–sea breeze or the ITCZ?, Journal of Earth System Science, 127, 5, 2018.

Gill, A.: Some simple solutions for heat-induced tropical circulation, Quarterly Journal of the Royal Meteorological Society, 106, 447–462,
1980.

Hazeleger, W., Severijns, C., Semmler, T., Ştefănescu, S., Yang, S., Wang, X., Wyser, K., Dutra, E., Baldasano, J. M., Bintanja, R., et al.:
35 EC-Earth: a seamless earth-system prediction approach in action, Bulletin of the American Meteorological Society, 91, 1357–1363, 2010.

Hazeleger, W., Wang, X., Severijns, C., Ştefănescu, S., Bintanja, R., Sterl, A., Wyser, K., Semmler, T., Yang, S., Van den Hurk, B., et al.:
EC-Earth V2. 2: description and validation of a new seamless earth system prediction model, Climate dynamics, 39, 2611–2629, 2012.

Hsu et al.: Land–ocean asymmetry of tropical precipitation changes in the mid-Holocene, Journal of Climate, 23, 4133–4151, 2010.

Kathayat, G., Cheng, H., Sinha, A., Yi, L., Li, X., Zhang, H., Li, H., Ning, Y., and Edwards, R. L.: The Indian monsoon variability and civilization changes in the Indian subcontinent, Science advances, 3, e1701 296, 2017.

Laskar, A. H., Yadava, M., Ramesh, R., Polyak, V., and Asmerom, Y.: A 4 kyr stalagmite oxygen isotopic record of the past Indian Summer

5   Monsoon in the Andaman Islands, Geochemistry, Geophysics, Geosystems, 14, 3555–3566, 2013.

Madec, G.: NEMO, the ocean engine, Note du Pole de modelisation, Institut Pierre-Simon Laplace (IPSL), France, No 27 ISSN No 1288–1619, 2008.

Merlis et al.: Hadley circulation response to orbital precession. Part II: Subtropical continent, Journal of Climate, 26, 754–771, 2013.

Neelin, J. D. and Held, I. M.: Modeling tropical convergence based on the moist static energy budget, Monthly Weather Review, 115, 3–12,

10   1987.

Patnaik et al.: Indian monsoon variability at different time scales: marine and terrestrial proxy records, 2012.

Ramesh, R.: High resolution Holocene monsoon records from different proxies: An assessment of their consistency, Current Science, pp. 1432–1436, 2001.

Sterl, A., Bintanja, R., Brodeau, L., Gleeson, E., Koenigk, T., Schmith, T., Semmler, T., Severijns, C., Wyser, K., and Yang, S.: A look at the

15   ocean in the EC-Earth climate model, Climate Dynamics, 39, 2631–2657, 2012.

Tuenter et al.: The response of the African summer monsoon to remote and local forcing due to precession and obliquity, Global and Planetary Change, 36, 219–235, 2003.

Valcke, S. and Morel, T.: OASIS and PALM, the CERFACS couplers, Tech. rep., Tech. rep., CERFACS, 2006.

Wang et al.: Millennial-and orbital-scale changes in the East Asian monsoon over the past 224,000 years, Nature, 451, 1090–1093, 2008.

20   Wang, X., Auler, A. S., Edwards, R., Cheng, H., Ito, E., Wang, Y., Kong, X., and Solheid, M.: Millennial-scale precipitation changes in southern Brazil over the past 90,000 years, Geophysical Research Letters, 34, 2007.

Zhang et al.: Holocene Asian monsoon evolution revealed by a pollen record from an alpine lake on the southeastern margin of the Qinghai–Tibetan Plateau, China, Climate of the Past, 12, 415–427, 2016.

Zhao, Y. and Harrison, S.: Mid-Holocene monsoons: a multi-model analysis of the inter-hemispheric differences in the responses to orbital

25   forcing and ocean feedbacks, Climate Dynamics, 39, 1457–1487, 2012.

Table 1. The orbital configuration used for the extremes in precession, Precession minima: P_{min}, Precession maxima: P_{max} and the pre-industrial. 'e' represents eccentricity, δ is the tilt and ω is the longitude of perihelion. The values of these have been chosen, based on the extremes in the precession parameter $esin(\pi + \omega)$, that have occurred in the last 1 Myrs. Pre-industrial values are shown for comparison.

	e	δ (°)	ω (°)
Pre-Industrial	0.017	23.45	282.04
P_{min}	0.056	22.08	95.96
P_{max}	0.058	22.08	273.5

Table 2. This table lists all the regions used in this article, and provides there corresponding co-ordinates.

Region	Co-ordinates
Northern tropics	(0^oN-30^oN; 0^oE-360^oE)
Southern tropics	(30^oS- 0^oN; 0^oE-360^oE)
Central India	(15^oN-25^oN; 73^oE- 83^oE)
Bay of Bengal	(10^oN-20^oN; 85^oE- 95^oE)
Arabian Sea	(5^oN-15^oN; 60^oE- 70^oE)
N. Africa	(5^oN-15^oN; 20^oW- 0^oE)
Brazil	(20^oS-10^oS; 70^oW- 50^oW)
South Atlantic	(20^oS-10^oS; 30^oW- 0^oE)
South Africa	(20^oS-10^oS; 15^oE- 35^oE)
North Australia	(25^oS-15^oS; 130^oE-140^oE)
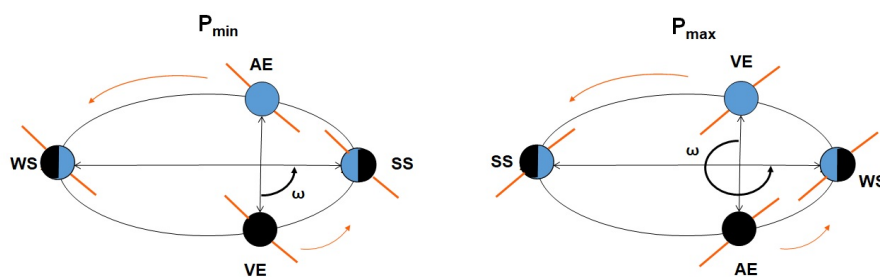
Figure 1. The schematic shows the orbital configuration of minimum precession (P_{min}) and maximum precession (P_{max}). In P_{min}, summer solstice (SS) takes place at perihelion, while in P_{max}, winter solstice (WS) coincides with the perihelion. AE and VE are the Autumn and Vernal Equinoxes respectively.
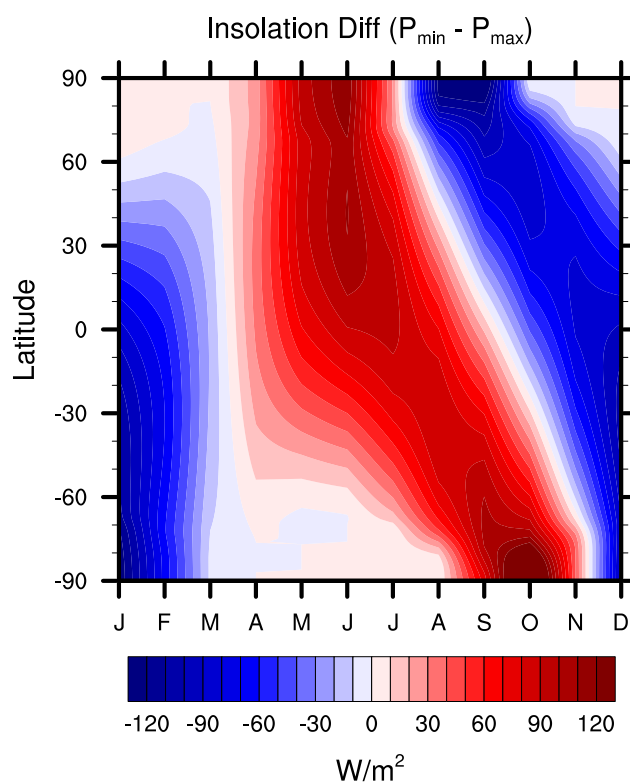
Figure 2. The difference in the incoming solar radiation at the top of atmosphere, between P_{min} and P_{max} as a function of latitude and month. This shows that insolation is higher during northern summer and lower during the northern winter in P_{min} compared to P_{max}.
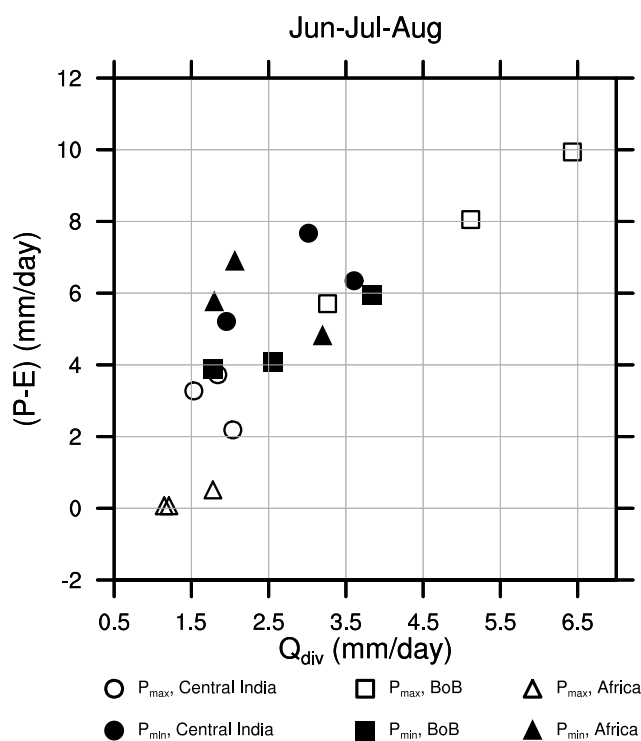
Figure 3. This figure shows the dependence of (P-E) on Q_{div} for three regions: Central India (15^oN-25^oN; 73^oE-83^oE), Bay of Bengal (10^oN-20^oN; 85^oE-95^oE) and Africa (5^oN-15^oN; 20^oW-25E^o). The scatter has been made for Jun-Jul-Aug separately. The hollow and filled symbols correspond to P_{max} and P_{min} respectively. (P-E) is directly proportional to Q_{div}.
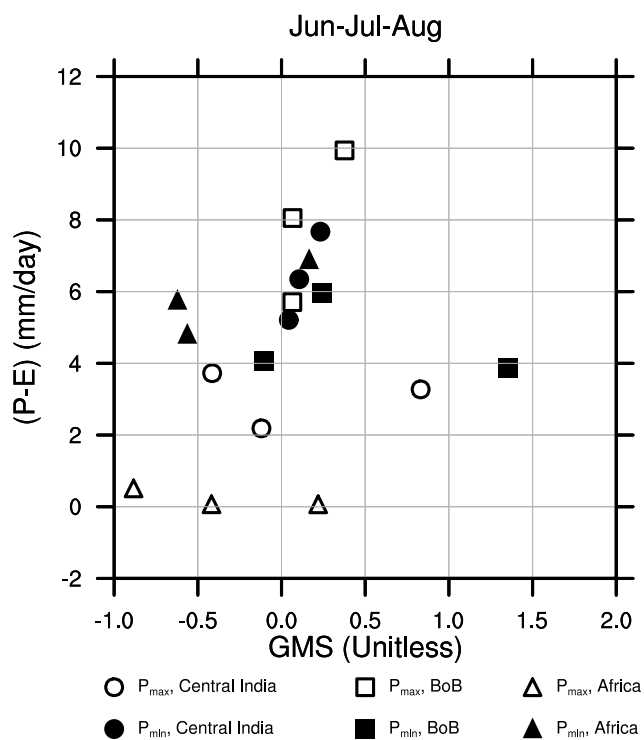
Figure 4. Same as figure (5), except that the x-axis is GMS. Negative values of GMS indicates that advection terms, which had been neglected, are significant.
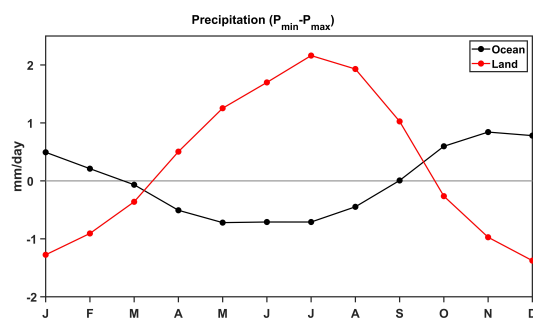
Figure 5. The difference in precipitation (P_{min}-P_{max}) for tropical land and ocean taken separately (30°S - 30°N). This shows the asymmetric response of the land and oceans to precessional forcing.
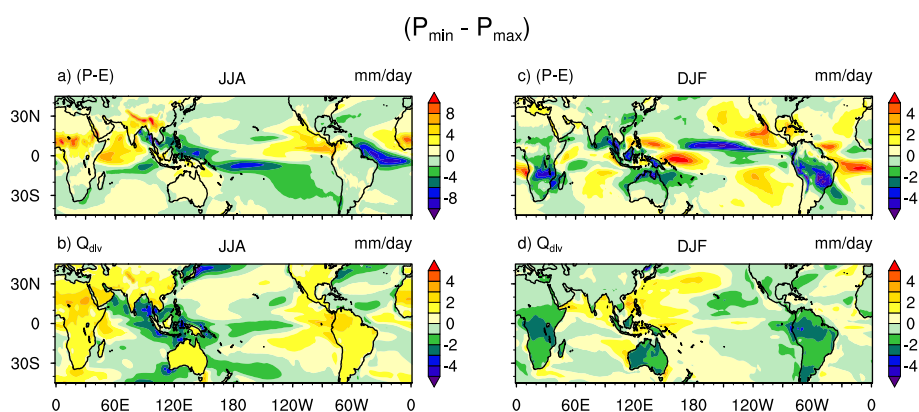
Figure 6. The figure shows difference in (P-E) (top panels **(a)** and **(c)**) and Q_{div} (bottom panels **(b)** and **(d)**). The left panels are for JJA and the right panels for DJF.
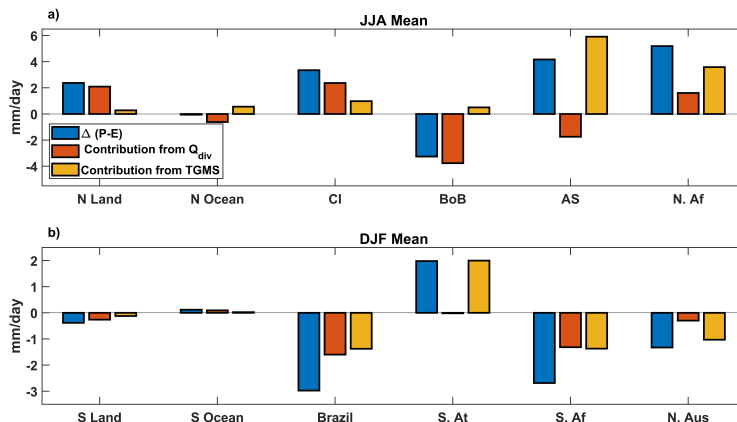
Figure 7. The bar chart shows the contribution of Q_{div} and TGMS to the changes in (P-E). The top panel **(a)** is for JJA and regions in Northern Hemisphere, while the bottom panel **(b)** is for regions in Southern Hemisphere and during DJF. The blue stick is the change in (P-E), while red and orange sticks represent the contribution from Q_{div} and TGMS. The abbreviations used in the top panel **(a)**, **N Land**: Northern tropics: land only, **N Ocean**: Northern tropics: Ocean only, **CI**: Central India, **BoB**: Bay of Bengal, **AS**: Arabian sea and **N. Af**: North Africa. and in the bottom panel **(b)**, **S Land**: Southern tropics: land only, **S Ocean**: Southern tropics: ocean only, **S. At**: South Atlantic, **S. Af**: South Africa. Refer to table 2 for the co-ordinates of these regions.
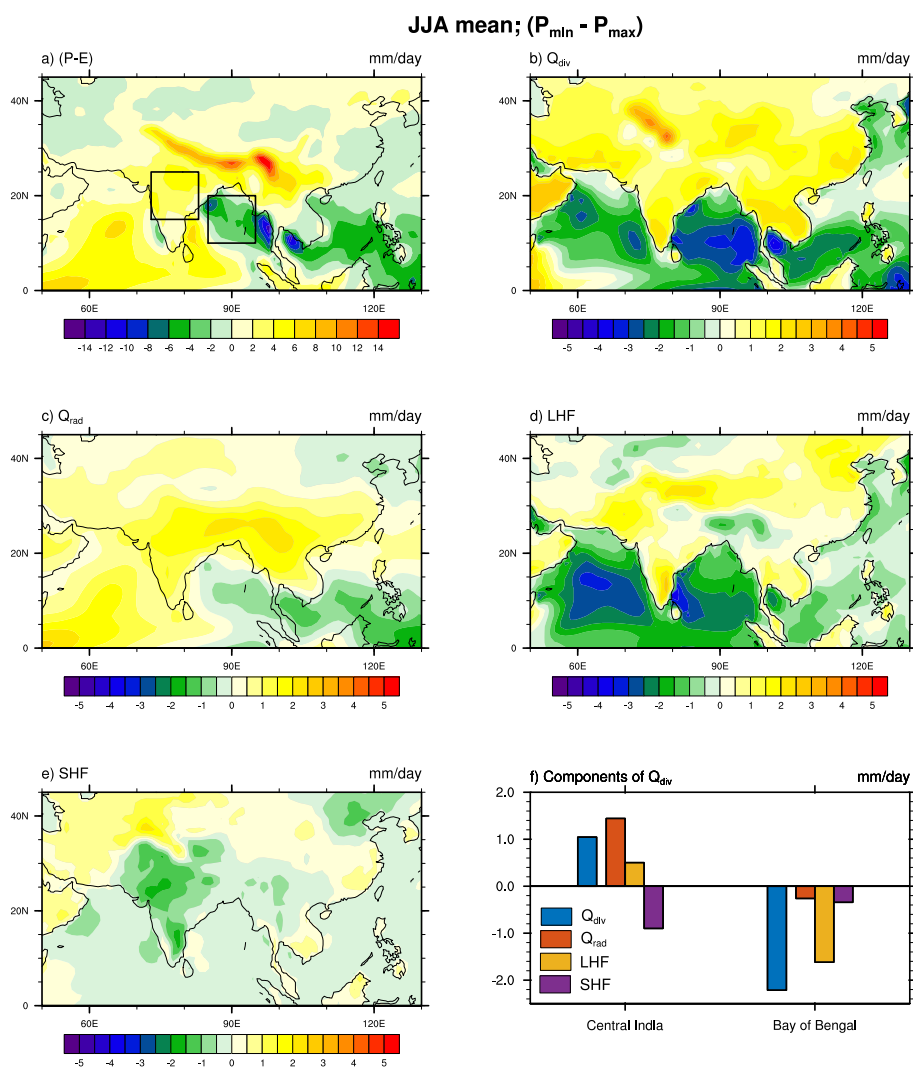
Figure 8. Shows the JJA mean difference (P_{min}-P_{max}), in **(a)** (P-E), **(b)** Q_{div}, **(c)** Q_{rad}, **(d)** Latent Heat Fluxes, **(e)** Sensible Heat Fluxes. The two boxes shown in **(a)**, are the regions chosen for this study: Central India (15^oN-25^oN; 73^oE-83^oE) and Bay of Bengal (10^oN-20^oN; 85^oE-95^oE). **(f)** shows the decomposition of Q_{div} into radiative, latent and sensible heat fluxes for the two regions. The blue bar is the change in Q_{div}, red: change in Q_{rad}, orange: change in latent heat fluxes and purple: change in sensible heat fluxes.
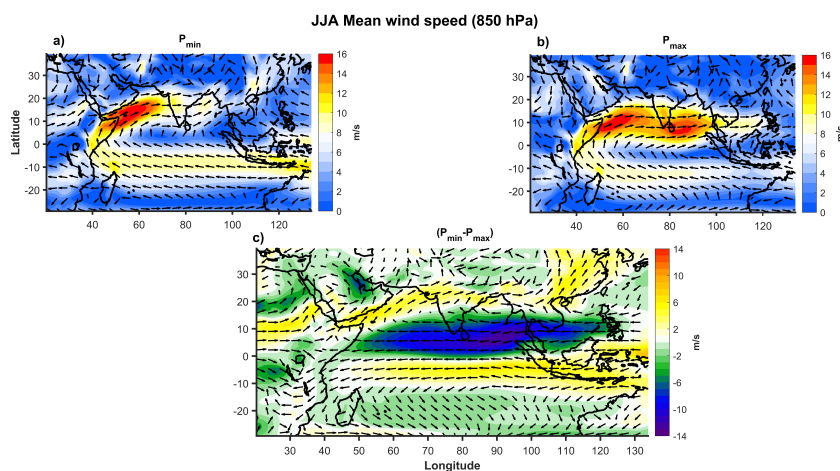
Figure 9. Top panels **(a)** and **(a)** show the JJA mean windspeed (850 hPa) in shading with unit vectors indicating direction for P_{min} and P_{max} respectively. The bottom panel **(c)**, shows the difference in winds (850 hPa). As can be seen from **(c)**, 40° E longitude has a convergence at equator and cyclonic circulation over the Middle-East. An anti-cyclonic circulation exists in the southern hemisphere over Madagasar. This is similar to the response of an atmosphere to equatorial plus off-equatorial heating (Gill, 1980)
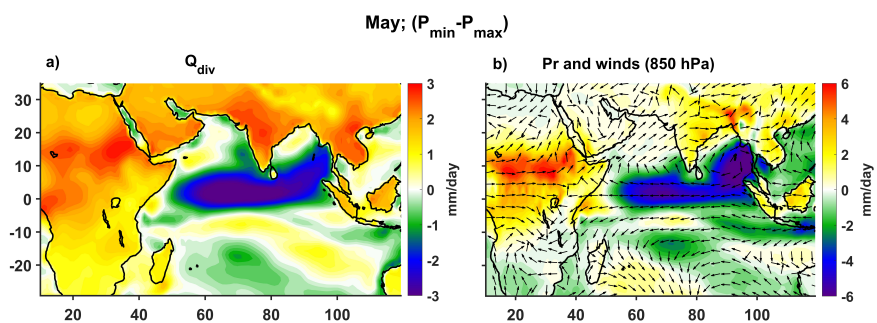
Figure 10. The difference between P_{min} and P_{max} in **(a)**, Q_{div} and **(b)**, Precipitation along with unit vectors indicating change in wind direction, for the month of May. This shows that, the large increase in Q_{div} over Africa causes an early onset of African monsoon. Thus influencing the winds over equatorial Indian Ocean.
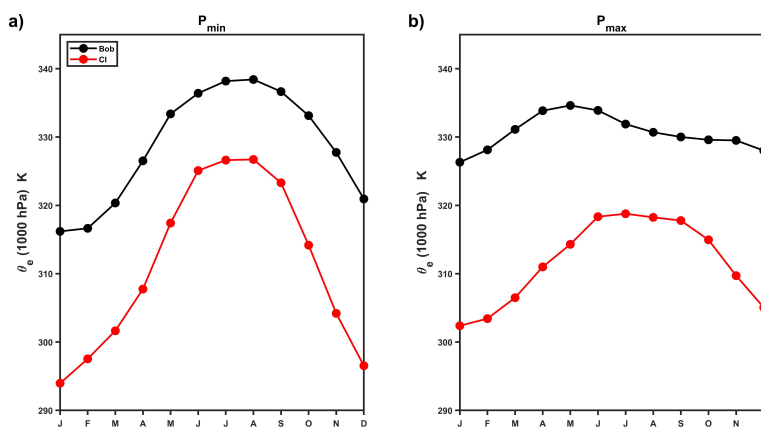
Figure A1. The plot shows the seasonal cycle of near surface equivalent potential temperature for India and BoB in the, **(a)** P_{min} configuration, and **(b)** P_{max}